Hybrid Model Predictive Control for Crosswind Stabilization of Hybrid Airships

Julian F. M. Foerster, Mohamed K. Helwa, Xintong Du, and Angela P. Schoellig

Abstract A hybrid airship is an aerial vehicle that generates lift by leveraging both buoyancy and aerodynamic principles. The operation of such a vehicle can be limited by its high susceptibility to crosswinds during taxiing, take-off and landing. With the goal to mitigate this issue, this paper proposes a novel controller design for a stabilization system consisting of wing tip thrusters. Due to the response of the vehicle to wind disturbances (e.g. lifting off a wheel during taxiing), modeling it as a hybrid dynamical system is appropriate. A novel, customized hybrid model predictive control (MPC) scheme is proposed for crosswind stabilization. As shown in simulation as well as in experimental results in controlled and realistic environments, the proposed control scheme succeeds in stabilizing the vehicle despite artificial or actual wind disturbances, even in scenarios where simple linear MPC fails. Simultaneously, our approach is computationally efficient enough to run on an onboard computer.

1 Introduction

Hybrid airships are heavier-than-air vehicles that generate a majority of their lift using buoyancy which is caused by a helium inflated wing-shaped envelope [1]. Resulting properties are a high energy efficiency during operation and short take-off and landing distances. Therefore, hybrid airships are very suitable for a number of logistics applications with remote origins and/or destinations, including supplying remote mines, disaster relief missions or, in general, supplying remote but inhabited

The authors are with the Dynamic Systems Lab (www.dynsyslab.org), University of Toronto Institute for Aerospace Studies, Canada. M. K. Helwa is also with the Electrical Power and Machines Department, Cairo University, Egypt. E-mail: {julian.forster, mohamed.helwa, xintong.du}@robotics.utias.utoronto.ca, schoellig@utias.utoronto.ca.

This work was partially supported by the Zeno Karl Schindler Foundation and the Natural Sciences and Engineering Research Council of Canada (NSERC).

locations with various goods [2]. However, the range of the vehicles' safe operating conditions can be limited due to a high susceptibility to crosswinds during taxiing, take-off and landing, which occurs due to the large surface area of the wing envelope. In the worst case, crosswind can lead to the vehicle tipping over.

The goal of this work is to design and implement an automatic counter-gust system (CGS) that stabilizes a hybrid airship despite wind disturbances during ground operations, to extend the set of safe operating conditions. This is achieved by estimating the vehicle attitude and current wind disturbance based on inertial measurement unit (IMU) data and then controlling thrusters that are mounted to the vehicle's wing tips to counteract the disturbance effect. The CGS controller aims to compute optimal control inputs, run autonomously without pilot intervention, be computationally efficient to run on onboard hardware, and be flexible regarding adaption to future hybrid airship designs.

All aircraft need to take precautions when taxiing under wind disturbances. For fixed-wing airplanes, this is done manually by the pilot using the control surfaces [3]. A wind stabilization system for hybrid airships is, for example, Lockheed Martin's air cushion landing system [4], but it is based on suction and thus only applicable when the vehicle is stationary. To the best of the authors' knowledge, there is no automatic wind stabilization system that operates during taxiing for any type of airship or fixed-wing plane.

In contrast, in-flight wind stabilization is quite common for small unmanned flying vehicles [5]. Often, wind disturbance estimates based on sensor data are computed and used to compensate for disturbances [5, 6]. In this paper, a similar approach is pursued, although vehicle size and CGS setup are unique in our case. More importantly, the approach in this paper is focussed on wind stabilization during ground operations as opposed to stabilization in flight.

Studying the hybrid aerial vehicle used for experiments in this paper led to modeling it as a hybrid dynamical system. Furthermore, we use predictive control for its ability to optimize the behavior over a prediction horizon. However, most common approaches to *hybrid model predictive control* (HMPC) are not suitable for our application due to their high computational complexity [7] or the lack of flexibility of explicit HMPC methods [8, 9]. A very recent approach allows to run nonlinear MPC faster than realtime, using quasi-translations [10]. However, it is based on the assumption that future predictions are almost perfect, which is violated in our case, given that wind disturbances are hard to predict. Therefore, a novel, customized HMPC scheme is proposed in Section 2.4, which is the main contribution of this paper.

2 Technical Approach

In this section, the methodology of the CGS design is detailed. Due to space constraints, emphasis is placed on the required estimation and control algorithms.

2.1 Physical Setup

In this paper, a CGS is designed, implemented and evaluated on a 4-meter wingspan unmanned hybrid airship. Figure 1 visualizes the physical setup of the vehicle and the CGS. The vehicle body mainly consists of an inflated wing envelope and two inflated pontoons. The tricycle undercarriage landing gear is composed of three wheels, two of which are mounted to the pontoons and one to the fuselage which is attached to the wing envelope. The CGS consists of sensors, a processor and thrusters. To maximize the control authority and thus the lever of the actuators, the thrusters are placed at the wing tips.

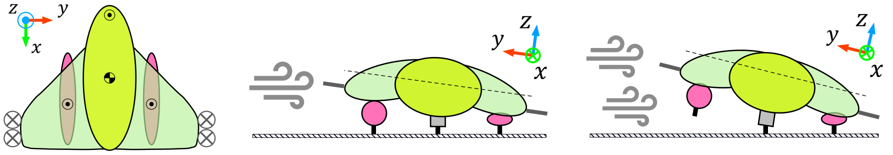

(a) Top-down view. The center of gravity is marked by ◕.

(b) Front view, vehicle in **mode 1** (all wheels have ground contact).

(c) Front view, vehicle in **mode 2** (back right wheel lifted).

Fig. 1: Schematic views of the hybrid airship studied in this paper, showing wing envelope (green), pontoons (magenta), landing gear positions (black circles), and wing tip thrusters (gray). The orientation of the body frame is shown for each view.

2.2 Hybrid System Model

Observations of the vehicle in operation led to differentiating three different vehicle dynamics, depending on the vehicle state. Therefore, the system is modeled as a hybrid dynamical system, consisting of a set of modes with continuous dynamics describing the system in each mode [11] (see Figure 2). As the yaw motion during ground operations is controlled manually by the vehicle's pilot, it is assumed to be constant at zero and thus not included in the vehicle state. The state consists of the roll and pitch angles (${}_1\alpha_x$ and ${}_1\alpha_y$) and their angular velocities (${}_1\omega_x$ and ${}_1\omega_y$), both in a body-fixed frame denoted by the leading subscript 1 and visualized in Figure 1. Frame 1's origin is located on the vehicle's roll axis. The state $\mathbf{x}$ is written as $\mathbf{x} = \left[{}_1\alpha_x \; {}_1\omega_x \; {}_1\alpha_y \; {}_1\omega_y\right]^T$. To obtain the dynamics $\dot{\mathbf{x}} = \left[{}_1\omega_x \; {}_1\dot{\omega}_x \; {}_1\omega_y \; {}_1\dot{\omega}_y\right]^T$, an expression for the angular acceleration in the body frame is needed. In the following, the dynamic modes used in this paper are introduced.

For disturbances below a certain magnitude, the vehicle's three wheels stay on the ground and its wing envelope rotates around its roll axis due to compression of

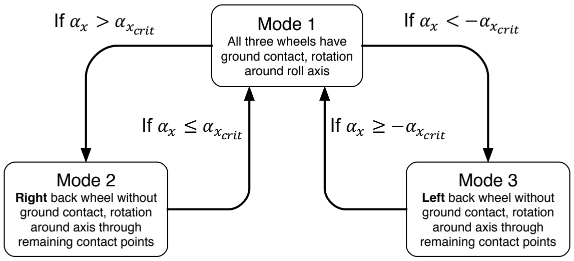
If $\alpha_x > \alpha_{x_{crit}}$
Mode 1
All three wheels have ground contact, rotation around roll axis
If $\alpha_x < -\alpha_{x_{crit}}$
If $\alpha_x \leq \alpha_{x_{crit}}$
If $\alpha_x \geq -\alpha_{x_{crit}}$
Mode 2
Right back wheel without ground contact, rotation around axis through remaining contact points
Mode 3
Left back wheel without ground contact, rotation around axis through remaining contact points

Fig. 2 Overview of the permissible mode switches and the conditions for a mode switch to happen. The occurrence of a switch only depends on the vehicle's roll angle α_x and the constant critical roll angle $\alpha_{x_{\text{crit}}}$.

the leeward pontoon. This is visualized in Figure 1b and referred to as mode 1. The angular acceleration expression for mode 1 is based on Euler's rotation equations for rigid bodies:

$$ {}_1\dot{\boldsymbol{\omega}} = \begin{bmatrix} {}_1\dot{\omega}_x \\ {}_1\dot{\omega}_y \\ * \end{bmatrix} = {}_1\boldsymbol{\theta}_{\text{wing}}^{-1} \left({}_1\boldsymbol{M} - \begin{bmatrix} {}_1\omega_x \\ {}_1\omega_y \\ 0 \end{bmatrix} \times \left({}_1\boldsymbol{\theta}_{\text{wing}} \begin{bmatrix} {}_1\omega_x \\ {}_1\omega_y \\ 0 \end{bmatrix} \right) \right), \tag{1} $$

where ${}_1\dot{\boldsymbol{\omega}}$ is the angular acceleration vector (the last component, marked with $*$, is discarded as justified above), ${}_1\boldsymbol{\theta}_{\text{wing}}$ is the inertia matrix of the wing only (without pontoons, fuselage and landing gear), ${}_1\boldsymbol{M}$ is the sum of all moments acting on the vehicle and $(.)^{-1}$ and $\times$ denote the matrix inverse and the cross product respectively. The moment ${}_1\boldsymbol{M}$ is composed as follows: ${}_1\boldsymbol{M} = {}_1\boldsymbol{M}_{\text{pontoons}} + {}_1\boldsymbol{M}_{\text{wind}} + {}_1\boldsymbol{M}_{\text{thrust}}$, ${}_1\boldsymbol{M}_{\text{pontoons}} = \left[-k_x \cdot {}_1\alpha_x - d_x \cdot {}_1\omega_x,\ -k_y \cdot {}_1\alpha_y - d_y \cdot {}_1\omega_y,\ 0\right]^T$, ${}_1\boldsymbol{M}_{\text{wind}} = {}_1\boldsymbol{b}_g \times (\boldsymbol{R}_{I1}^T\ {}_I\boldsymbol{F}_{\text{wind}})$ and ${}_1\boldsymbol{M}_{\text{thrust}} = \sum_{i=1}^4 ({}_1\boldsymbol{b}_g + \boldsymbol{R}_{1g}\ {}_g\boldsymbol{r}_{t,i}) \times \boldsymbol{R}_{1g}\ {}_g\boldsymbol{F}_{t,i}$, where ${}_1\boldsymbol{M}_{\text{pontoons}}$, ${}_1\boldsymbol{M}_{\text{wind}}$ and ${}_1\boldsymbol{M}_{\text{thrust}}$ are the moments exerted by pontoons, wind disturbance and wing tip thrusters, respectively, k_i and d_i denote spring and damping coefficients for axis i, ${}_1\boldsymbol{b}_g$ is the vector from the origin of frame 1 to the vehicle's center of mass (CoM), $\boldsymbol{R}_{I1}$ is the rotation matrix between frame 1 and the inertial frame, in which the wind disturbance force ${}_I\boldsymbol{F}_{\text{wind}}$ is expressed, $\boldsymbol{R}_{1g}$ is the rotation matrix between frame 1 and the body frame g with the origin at the CoM ($\boldsymbol{R}_{1g}$ is the identity matrix in this paper), ${}_g\boldsymbol{r}_{t,i}$ is the vector from the CoM to the ith wing tip thruster and ${}_g\boldsymbol{F}_{t,i}$ is the thrust produced by the ith thruster. The produced thrust is obtained via an experimentally determined static thrust map and the input command $\mathbf{u} = \left[u_1,\ u_2\right]^T$, where $u_1, u_2 \in [0,1]$ is the starboard/port input command, respectively. A command of zero means idle rotation, and a command of one means full thrust.

For higher disturbances, one of the back wheels can loose ground contact, which occurs at the *critical roll angle*. Consequently, the vehicle rotates around the axis passing through the remaining two contact points, which is visualized in Figure 1c and referred to as mode 2 or 3, depending on which back wheel is lifted. It is also possible that the front wheel lifts off. However, this behavior is typically related to disturbances other than wind (e.g. potholes) and therefore out of the scope of this paper. To formalize modes 2 and 3, new body fixed reference frames are introduced. Both have their origin in the contact point between front wheel and ground and the x-axis points towards the remaining back wheel contact point (the left one for mode

2 and the right one for mode 3). In the following, equations for mode 2 are given. The ones for mode 3 can be obtained analogously. Similar to mode 1, formalizing the dynamics in mode 2 requires the angular acceleration:

$$ {}_2\dot{\boldsymbol{\omega}} = {}_2\boldsymbol{\theta}^{-1}\left({}_2\boldsymbol{M} - \begin{bmatrix} {}_2\omega_x \\ 0 \\ 0 \end{bmatrix} \times \left({}_2\boldsymbol{\theta}\begin{bmatrix} {}_2\omega_x \\ 0 \\ 0 \end{bmatrix}\right)\right), \tag{2} $$

where the leading subscript denotes the reference frame for mode 2 introduced above and $\boldsymbol{\theta}$ is the inertia matrix of the whole vehicle. The sum of the moments acting in mode 2, denoted ${}_2\boldsymbol{M}$, is composed as follows: ${}_2\boldsymbol{M} = {}_2\boldsymbol{M}_{\text{wind}} + {}_2\boldsymbol{M}_{\text{thrust}} + {}_2\boldsymbol{M}_{\text{gravity}}$, ${}_2\boldsymbol{M}_{\text{gravity}} = {}_2\boldsymbol{b}_g \times (\boldsymbol{R}_{2I}\,{}_I\boldsymbol{F}_g)$. The moments ${}_2\boldsymbol{M}_{\text{wind}}$ and ${}_2\boldsymbol{M}_{\text{thrust}}$ are defined analogously to the respective moments in mode 1 and ${}_2\boldsymbol{b}_g$ is the vector from the origin of frame 2 to the CoM, $\boldsymbol{R}_{2I}$ is the rotation matrix between frame 2 and the inertial frame, and ${}_I\boldsymbol{F}_g$ is the gravity force, expressed in the inertial frame.

To make the models usable in a discrete time setting, the above continuous time models are linearized and discretized. The operating point for the linearization is the horizontal attitude with zero angular velocities for mode 1 and the critical roll angle with zero angular velocities for modes 2 and 3. Finally, the models for the separate modes are combined into a piecewise affine (PWA) formulation [12], which consists of the three linear discrete time models and for each mode a region of the state and input space in which it is active (see Figure 2).

2.3 State & Disturbance Estimation

The goal of the CGS controller is to control the wing tip thrusters to compensate for the effect of the disturbance. To achieve this, an estimate of the current disturbance is used by the MPC to account for it over the prediction horizon and to find an optimal control input. Based on our previous work [13], the best way to get a disturbance estimate that offers a reasonable trade-off between accuracy, simplicity and cost is to deduce it from IMU data using a Kalman filter. Other solutions to obtain a disturbance estimate, like adding an anemometer, turned out to be too expensive or technically infeasible. Therefore, apart from estimating the vehicle state $\mathbf{x}[k]$ at a discrete time k, the Kalman filter estimates the current disturbance $d[k]$ by using an augmented state $\tilde{\mathbf{x}}[k] = [\mathbf{x}^T[k], d[k]]^T$. Note that since the main dynamics cause a roll motion, the disturbance ${}_I\boldsymbol{F}_{\text{wind}}$ is reduced to its y component, which is denoted by $d[k]$.

As process model, the system model is used for the state $\mathbf{x}[k]$ (see Section 2.2) and the disturbance is modeled as $d[k+1] = d[k] + w[k]$, where $w[k] \sim \mathscr{N}(0, \sigma_d^2)$ is white Gaussian noise with zero mean and standard deviation σ_d. The disturbance model assumes that the disturbance is approximately constant over one sampling interval, which is a common assumption for short term wind prediction [14].

Despite the fact that the vehicle is modeled as a hybrid system (as introduced in Section 2.2), a Kalman filter for linear systems is used. In each time step, it uses the model for the mode that the vehicle was in at the last time step according to the previous state estimate. This procedure introduces a small error if a mode switch occured during the current sampling interval. The error is compensated for in subsequent Kalman filter executions.

2.4 Customized Hybrid Model Predictive Control

To control the CGS, MPC is used, mainly due to its prediction capabilities, intuitive tuning, and seamless integration of state and input constraints. Since the system model is hybrid as discussed in Section 2.2, HMPC must be used. For HMPC, the optimization problem that must be solved at each time step is a *mixed integer program* (MIP) [15], which is computationally expensive to solve. A preliminary experimental analysis of the system showed that a sampling frequency of at least 10 Hz and a prediction horizon of at least 1 second is needed for adequate performance of the CGS. A benchmark study by Corona and De Schutter [7] shows that solving HMPC for such a long prediction horizon within such a short sampling period is not achievable with today's MIP solvers. Therefore and as the main contribution of this paper, a customized HMPC scheme is proposed that respects the hybrid nature of the vehicle dynamics, and simultaneously can be executed online on a microprocessor.

The proposed, customized HMPC strategy was designed by starting from a brute force approach to HMPC and, subsequently, reducing the necessary computations significantly based on insights into the system behavior. The brute force approach solves at each time step one quadratic program (QP) for each possible switching sequence. A switching sequence is a sequence of modes over the prediction horizon. If a switching sequence is given, the optimization problem to be solved by the controller is a QP. The optimization problem corresponding to a given switching sequence ϑ can be stated as

$$\begin{aligned}
\mathbf{U}^* = \arg\min_{\mathbf{U}} \quad & J(\mathbf{X},\mathbf{U}) = \sum_{i=1}^{i=N_p} \left(\mathbf{x}_{k+i}^T \mathbf{Q} \mathbf{x}_{k+i}\right) + \\
& \sum_{i=0}^{i=N_p-1} \left(\mathbf{u}_{k+i}^T \mathbf{R} \mathbf{u}_{k+i} + (\delta \mathbf{u}_{k+i})^T \mathbf{S} (\delta \mathbf{u}_{k+i})\right) \\
\text{s.t.} \quad & \mathbf{x}_{k+i+1} = \mathbf{L}_{j(i)} + \mathbf{A}_{j(i)} \mathbf{x}_{k+i} + \mathbf{B}_{j(i)} \mathbf{u}_{k+i} \\
& \mathbf{x}_k = \hat{\mathbf{x}}_k \\
& j(i) = \vartheta(i) \\
& \mathbf{X} = (\mathbf{x}_{k+1}^T, \ldots, \mathbf{x}_{k+N_p}^T)^T, \mathbf{U} = (\mathbf{u}_k^T, \ldots, \mathbf{u}_{k+N_p-1}^T)^T \\
& i \in \{0, \ldots, N_p - 1\},
\end{aligned} \tag{3}$$

where J is the cost function, $\delta \mathbf{u}_i = \mathbf{u}_i - \mathbf{u}_{i-1}$, $\mathbf{Q}$, $\mathbf{R}$ and $\mathbf{S}$ are weight matrices of appropriate dimensions for the state, the input and the input change $\delta \mathbf{u}$, respectively,

$\{\mathbf{A}_j, \mathbf{B}_j, \mathbf{L}_j\}$ are the matrices of the affine state space model active in mode j, $\mathbf{x}_i$ and $\mathbf{u}_i$ are state and input at time step i and N_p is the prediction horizon length.

With 3 modes, the number of switching sequences for the brute force approach is 3^{N_p}. For $N_p = 15$ as required for our system, the brute force approach would be to solve 14 348 907 QPs per time step, which is computationally infeasible under the constraints of the onboard processor. Instead, only switching sequences with a single mode switch are considered by our proposed controller. Consequently, the number of QPs that need to be solved at each time step is reduced to $N_p + 1$. This simplification is based on experimental observations and the intuition that more than one mode switch during the short prediction horizon (around 1 sec) is very rare due to the high inertia of the vehicle.

The proposed algorithm (executed once per sampling period) is shown in Algorithm 1. As inputs, it takes a state estimate $\hat{\mathbf{x}}$ (consisting of the roll and pitch angles and angular velocities) and a scalar disturbance estimate $\hat{d}$. Then, for each possible switching sequence ϑ with at most one mode switch, a QP is formulated and solved. Finally, the control input $\mathbf{u}$ is selected for which the cost c accumulated over the prediction horizon is smallest.

Algorithm 1 Customized HMPC scheme. *Inputs*: state estimate $\hat{\mathbf{x}}$, disturbance estimate $\hat{d}$. *Output*: optimal control input $\mathbf{u}^*$.

```
$m \leftarrow$ getCurrentMode($\hat{\mathbf{x}}$)
if $m = 1$ then                          ▷ $m$: current mode
    if $\hat{\mathbf{x}}^{(1)} \geq 0$ then               ▷ Roll angle $\geq 0$
        $n \leftarrow 2$                     ▷ $n$: anticipated mode
    else
        $n \leftarrow 3$
else
    $n \leftarrow 1$
$i_{\text{switch}} \leftarrow N_p$                    ▷ $i_{\text{switch}}$: switching index
$c^* \leftarrow \infty$                        ▷ $c^*$: lowest cost so far
while $i_{\text{switch}} \geq 0$ do                ▷ $\vartheta$: switching seq.
    $\vartheta \leftarrow (\underbrace{m,\ldots,m}_{i_{\text{switch}}}, \underbrace{n,\ldots,n}_{N_p - i_{\text{switch}}})$
    $(\mathbf{u}, c) \leftarrow$ solveQP($\vartheta, \hat{\mathbf{x}}, \hat{d}$)
    if $c < c^*$ then
        $c^* \leftarrow c$
        $\mathbf{u}^* \leftarrow \mathbf{u}$
    $i_{\text{switch}} \leftarrow i_{\text{switch}} - 1$
return $\mathbf{u}^*$
```

3 Simulation Results

In a first simulation, which is shown in Figure 3a, the proposed controller is compared to linear MPC (LMPC), which assumes that mode 1 is active throughout the whole state space. The same disturbance is applied for both controllers. While the vehicle tips over when controlled by LMPC, the proposed CHMPC stabilizes the vehicle successfully. The reason is the control input issued by each controller. Because the CHMPC considers the chance of an upcoming mode switch, it anticipates the risk of leaving mode 1. Thus, it increases the thrust earlier than LMPC, which ensures that the vehicle is stabilized successfully.

Furthermore, the performance of CHMPC for the case when more than one mode switch occurs during the prediction horizon is investigated. For this purpose, another controller is introduced: the brute force hybrid MPC (BFHMPC). At each time step, it solves one QP for each possible switching sequence (as defined in Section 2.4). As shown in Figure 3b, the performance of the proposed CHMPC scheme is very similar to the performance of BFHMPC, despite the fact that CHMPC only anticipates one mode switch.

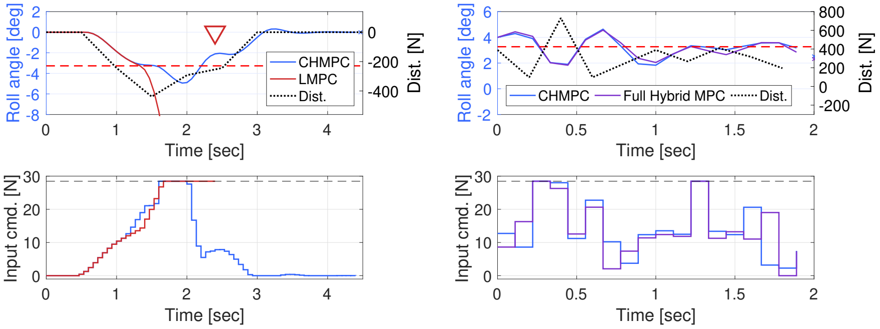

(a) Roll angles during a simulation comparing the proposed customized HMPC (CHMPC) strategy to a standard linear MPC (LMPC). The red dashed line represents the border between mode 1 (above) and mode 3 (below). The LMPC does not manage to stabilize the vehicle against the applied disturbance (red triangle marks tipping over) while the CHMPC does. The reason for this is that the CHMPC anticipates mode 3 and thus increases the thrust earlier to avoid it (see lower plot between 1 and 1.5 sec).

(b) Comparison between the brute force HMPC and the proposed strategy. The disturbance in this example is chosen to force more than one mode switch during the prediction horizon length of one second. Despite the fact that CHMPC is computationally significantly more efficient than brute force HMPC, their performance is comparable.

Fig. 3: Simulation results.

4 Experiments

This section gives details on how the proposed control scheme was tested in experiments and on the results achieved in these experiments.

4.1 Experimental Setup

The main goals of the experiments are to assess the CGS' performance in practice as well as to compare the proposed customized HMPC strategy with the simpler linear MPC approach, which only considers mode 1. As shown in Figure 3a, simulations predict that the proposed control strategy outperforms linear MPC in certain situations. What remains is to assess if this can also be observed in practice. With these goals in mind, experiments in two different settings were carried out:

First, **indoor experiments** were conducted with the goal to verify estimator accuracy and controller performance in an environment that allows full control over the disturbance acting on the vehicle. This is achieved by attaching known weights to one end of a rope, which is diverted using a pulley system and attached to the vehicle at the other end (see Figure 4a). The rope is diverted so that it exerts a horizontal force on the vehicle to closely match the effect wind disturbances have.

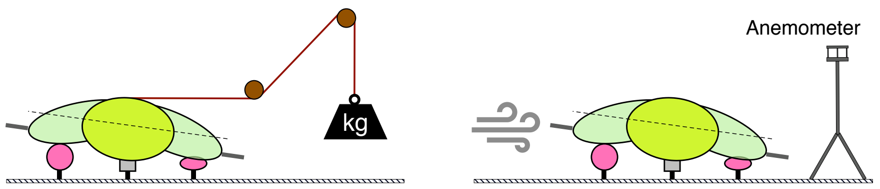

(a) **Indoor experiments**. The vehicle is deflected around its roll axis using a rope-pulley-system and different weights.

(b) **Outdoor experiments**. Realistic wind disturbances act on the vehicle. The current wind speed is measured using an anemometer.

Fig. 4: Schematics showing the indoor and outdoor experimental setups.

Second, **outdoor experiments** were carried out to assess the overall system performance under realistic weather conditions. In order to quantify the disturbance acting on the vehicle at each time step, an ultrasonic anemometer was used during all outdoor experiments (see Figure 4b). It has a sampling rate of 10 Hz and an accuracy of $\pm 2\%$ below $30\ \mathrm{m/s}$ and $\pm 3\%$ between $30\ \mathrm{m/s}$ and $70\ \mathrm{m/s}$. Note that the wind speed measurements from the anemometer are solely used as ground-truth for the Kalman filter disturbance estimate and they are not available to the controller.

For these experiments, both the controller and the estimator are implemented in C++, using ROS to manage communication. The algorithms are executed on a *Raspberry Pi 3 Model B* with a *QuadCore* 1.2 GHz CPU and 1 GB of RAM. To seize the full potential of the multi-core hardware, the execution of the control algorithm is parallelized. With this setup, a sampling frequency of 15 Hz and a prediction horizon of 15 time steps is achievable and was selected for all experiments. Data from six gyroscopes and six accelerometers is used as input to the estimator. Two of each are placed on each wing tip and the remaining two accelerometers and gyroscopes are placed on top of the wing envelope above the roll axis in the center of the vehicle.

4.2 Experimental Results and Insights

The estimation accuracy during an indoor experiment is shown in the center plot in Figure 5a. Both in the case with and without CGS, the applied disturbance is estimated accurately using the proposed Kalman filter.

As illustrated in the top plot in Figure 5a, the controller reduces the steady-state roll angle by 66% to 68%. The angle is not reduced to zero because the maximum thrust is not large enough to completely counteract the applied disturbance. In the case without CGS, the vehicle gets very close to a mode switch, which corresponds to one wheel lifting off the ground. A slightly higher disturbance would trigger a mode switch and therefore compromise safe taxiing. In contrast, when the vehicle is controlled by the CGS, the thrusters' capabilities are used optimally to compensate for the disturbance and keep the vehicle in the safe mode 1.

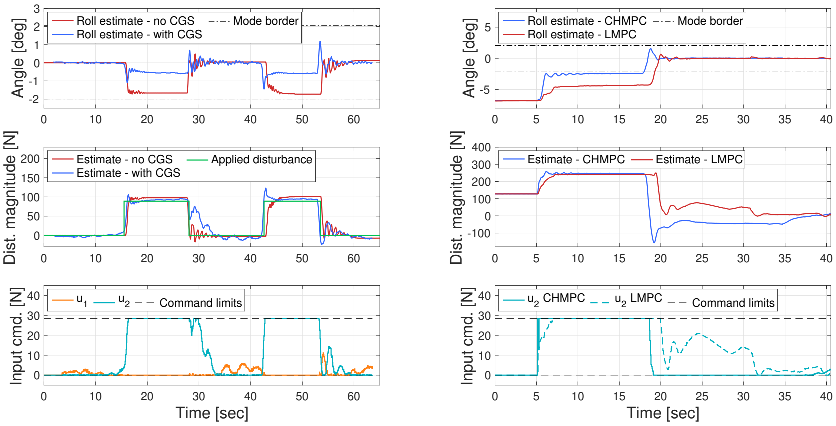

(a) The cases with and without CGS are compared for the case when a square disturbance (20 lb) is applied and released twice. With CGS, the resulting roll angle is reduced by 66% to 68% compared to the case without CGS.

(b) Comparison of proposed controller (CHMPC) to linear MPC (LMPC). The vehicle is manually deflected to a roll angle of 6° (back left wheel raised) before the disturbance is applied and the CGS is activated, both happening simultaneously at 5 sec. The CHMPC anticipates the risk of being in mode 3 and therefore increases the control command faster. Around 18 sec, the disturbance is removed.

Fig. 5: Results from **indoor experiments**.

During further indoor experiments, the proposed HMPC was compared to linear MPC (see Figure 5b). For this purpose, the vehicle is manually deflected around its roll axis before the disturbance is applied and the CGS is activated. Then, the controller activation and disturbance application happen simultaneously (after 5 seconds in Figure 5b). This procedure allows to observe the controller behavior when the vehicle is not in mode 1, which is where the strength of the proposed controller becomes apparent. The observed performance is similar to what was encountered in the simulation results (Section 3): while the LMPC ramps up the counteracting control command gradually, the CHMPC correctly recognizes the risk of being in mode 3 (i.e. having one wheel raised). As a result, the CHMPC stabilizes the vehicle at a roll angle that is 44% lower than the roll angle achieved by the LMPC. Note that the rope pulley system used in the indoor experiments introduces some friction, which damps any vehicle motion. Without this damping effect, the LMPC is less likely to prevent the vehicle from tipping over.

Finally, during the outdoor experiments, the CGS successfully stabilized the vehicle against wind gusts up to 9 m/s (32.4 km/h), which is the highest wind speed that was observed while the controller was active. The corresponding data is shown in Figure 6a. Note that the controller manages to keep the roll angle below the critical roll angle (at which a mode switch would occur) at all times. During a run without CGS, a gust with a speed of 10 m/s managed to flip the vehicle over (see Figure 6b at 68 sec). Even before that, at 54 and 59.5 seconds, and at lower wind speeds the roll angle exceeds the critical roll angle. This illustrates that the CGS is capable of increasing the hybrid airship's stability under realistic crosswind conditions, within the limits of the actuators.

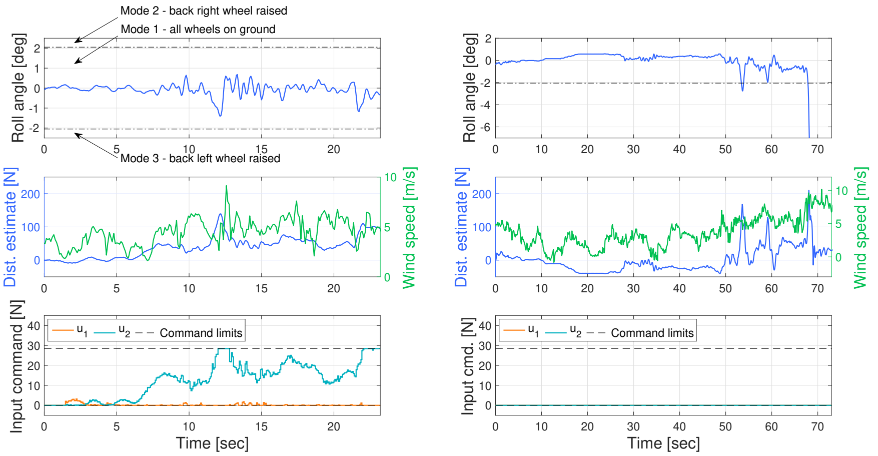

(a) Roll angle estimate, disturbance estimate, crosswind speed measurements and control inputs during an outdoor experiment. There is a correlation between disturbance estimate and wind speed, see for example spike around 13 sec. The CGS manages to stabilize the vehicle against a wind gust of up to 9 m/s.

(b) Data from an experiment run in which the CGS was disabled. At 69 sec, the wind speed (green curve) increases to above 10 m/s. As a result, the vehicle flips over.

Fig. 6: Results from **outdoor experiments**.

5 Conclusions

In this paper, the design and experimental validation of a counter gust system for a hybrid airship were discussed. For this purpose, the vehicle is modeled as a hybrid dynamical system, which challenges the controller design. To address this, the main contribution of this paper is a customized hybrid MPC scheme that, on the one hand, outperforms a linear MPC approach and, on the other hand, was proven to run in real time onboard the vehicle. Future work includes additional in-depth outdoor testing of the system under realistic wind conditions to further prove that the system is reliable in the real-world application it was designed for.

References

1. G. A. Khoury, *Airship Technology*, 2nd ed. Cambridge University Press, 2012.
2. Z. B. Jiron, "Hybrid Airships for Lift: A New Lift Paradigm and a Pragmatic Assessment of the Vehicle's Key Operational Challenges," Air University, Maxwell Air Force Base, Alabama, Tech. Rep. December, 2011.
3. *Airplane Flying Handbook*, U.S. Department of Transportation, Federal Aviation Administration, Flight Standards Service, 2016.
4. Lockheed Martin Corp., "Air Cushion Landing System," Accessed: 2018-04-20. [Online]. Available: https://www.lockheedmartin.com/en-us/news/features/2016/hovercraft-technology-help-people-remote-parts-of-world.html
5. S. Waslander and C. Wang, "Wind Disturbance Estimation and Rejection for Quadrotor Position Control," *AIAA Infotech@Aerospace Conference*, p. 1983, 2009.
6. Y. Demitri, S. Verling, T. Stastny, A. Melzer, and R. Siegwart, "Model-based Wind Estimation for a Hovering VTOL Tailsitter UAV," in *2017 IEEE International Conference on Robotics and Automation (ICRA)*, 2017, pp. 3945–3952.
7. D. Corona and B. De Schutter, "Adaptive Cruise Control for a SMART Car: A Comparison Benchmark for MPC-PWA Control Methods," *IEEE Transactions on Control Systems Technology*, vol. 16, no. 2, pp. 365–372, 2008.
8. R. Oberdieck and E. N. Pistikopoulos, "Explicit Hybrid Model-Predictive Control: The Exact Solution," *Automatica*, vol. 58, pp. 152–159, 2015.
9. N. Giorgetti, G. Ripaccioli, A. Bemporad, I. Kolmanovsky, and D. Hrovat, "Hybrid Model Predictive Control of Direct Injection Stratified Charge Engines," *IEEE/ASME Transactions on Mechatronics*, vol. 11, no. 5, pp. 499–506, 2006.
10. A. Maitland and J. McPhee, "Fast NMPC with Mixed-Integer Controls using Quasi-Translations," in *6th IFAC Conference on Nonlinear Model Predictive Control*, 2018.
11. S. Engell, G. Frehse, and E. Schnieder, *Modelling, analysis and design of hybrid systems*. Springer, 2003, vol. 279.
12. E. D. Sontag, "Nonlinear Regulation: The Piecewise Linear Approach," *IEEE Transactions on Automatic Control*, vol. 26, no. 2, pp. 346–358, 1981.
13. M. K. Helwa, A. Esser, and A. P. Schoellig, "Estimation-Based Model Predictive Control for Automatic Crosswind Stabilization of Hybrid Aerial Vehicles," *arXiv preprint arXiv:1810.00046 [cs.SY]*, 2018.
14. S. S. Soman, H. Zareipour, O. Malik, and P. Mandal, "A Review of Wind Power and Wind Speed Forecasting Methods with Different Time Horizons," in *North American Power Symposium*, 2010, pp. 1–8.
15. E. F. Camacho, D. R. Ramirez, D. Limon, D. Munoz de la Pena, and T. Alamo, "Model Predictive Control Techniques for Hybrid Systems," *Annual Reviews in Control*, vol. 34, pp. 21–31, 2010.